ACS ES&T Water

pubs.acs.org/estwater

Article

Assessing Phosphorus Loading Targets for Lake Erie Algal Blooms and Hypoxia under Climate Variability

Donald Scavia,* Yu-Chen Wang, and Daniel R. Obenour

Cite This: https://doi.org/10.1021/acsestwater.6c00002

Read Online

ACCESS | Metrics & More | Article Recommendations | Supporting Information

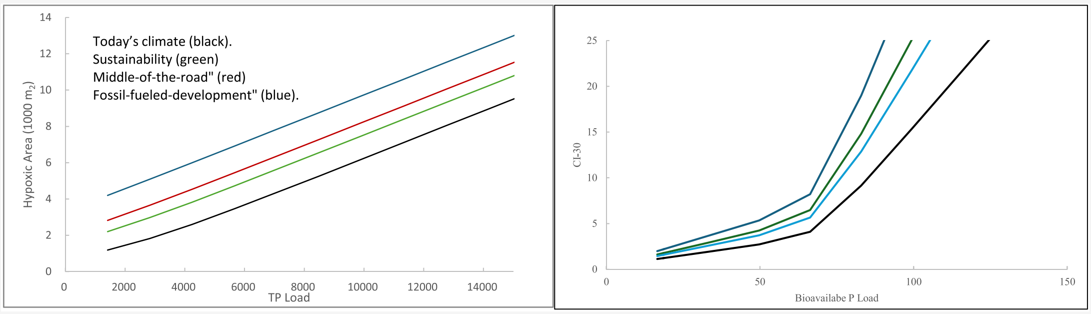

ABSTRACT: A decade ago, the United States and Canada revised Lake Erie's phosphorus loading targets to address increasing severity of western basin harmful algal blooms (HABs) and central basin hypoxia. To mitigate HABs, targets were set for spring (March−July) loads of total phosphorus (860 metric tonnes [MT]) and dissolved reactive phosphorus (186 MT) from the Maumee River. To raise the average central basin summer hypolimnetic dissolved oxygen concentration above 2 mg/L, annual total phosphorus (TP) load target of 6000 MT/year was established. We update, apply, and improve HAB and hypoxia models to re-evaluate load−response curves, estimate temporal lags, and quantify the influence of climate. Both models are developed within Bayesian frameworks to provide uncertainty quantification. Under the current climate, the HAB and hypoxia targets require a 21% reduction in the 2020−2024 average spring total bioavailable phosphorus (TBP) load, and an 18% reduction in the annual TP load. Once loading goals are achieved, we project an average lag of 7.0 and 9.0 years for hypoxia and HAB. Under moderate climate change, midcentury targets require a 38% reduction from today's spring TBP loads and a 45% reduction of annual TP load. Larger loading reductions will be required during wet years.

KEYWORDS: *harmful algal blooms, hypoxia, Bayesian models, Lake Erie, phosphorus loads*

■ INTRODUCTION

The United States and Canada revised Lake Erie phosphorus loading targets to address increasing severity of western-basin harmful algal blooms (HABs) and central-basin hypoxia.[1] To mitigate HAB severity, binational agreements recommended a spring (March−July) total phosphorus (TP) load of 860 mtric tonnes (MT) and a dissolved reactive phosphorus (DRP) load of 186 MT from the Maumee River. For central-basin hypoxia, annual TP load target of 6000 MT (aggregated across multiple river basins) was established with the expectation of raising the average August−September hypolimnetic dissolved oxygen concentration to at least 2.0 mg/L. Those target loads have not changed and were guided by data and models evaluated through 2014[2] and shaped by public engagement. To date, these loading targets have generally not been met.[3]

The targets and the supporting models were consistent with adaptive management frameworks[4] and recommendations from consensus workshops.[5] However, over a decade has passed since these goals were set. The scientific community now benefits from extended observational data sets, a suite of updated HAB and hypoxia models, increased understanding of the impacts of weather and climate, and new information regarding the impact of hypoxia on fisheries.[6−23] Consequently, it is necessary to update the models that establish relationships between watershed loads and water quality outcomes, as represented graphically by "load−response curves." Through this process, it is also possible to reassess the temporal lags associated with lake responses to changing watershed loads and to explicitly consider the influence of climate variability.

In this paper, we update, improve, and apply established western-basin HAB[24] and central-basin hypoxia[10] models using Bayesian frameworks. Both models are calibrated with

Received: January 1, 2026
Revised: June 19, 2026
Accepted: June 22, 2026

observational data extended through 2024. Furthermore, the HAB model structure is updated to include a temperature term to explicitly account for climate variability on the lake's response, complementing the temperature dependencies already represented in the hypoxia model. By applying these models, we provide credible intervals for all parameters, predictive response curves with rigorously quantified uncertainties, and estimated temporal lags in the lake's response following phosphorus load reductions. For both HABs and hypoxia, load–response curves are developed for current conditions as well as for future temperature projections associated with climate change.

■ METHODS

Study Site

The focus of this study is Lake Erie (Figure 1), specifically examining western-basin HABs and central-basin hypoxia.[1,2,25,26] The primary nutrient influencing the maximum HAB size in the western basin is the phosphorus load from the Maumee River.[27] For central-basin hypoxia, we aggregate the total phosphorus (TP) loads to both the western and central basins, including inputs from Lake Huron via the Detroit River. All model inputs and observational data are provided in the Supporting Information (Tables S1 and S2).

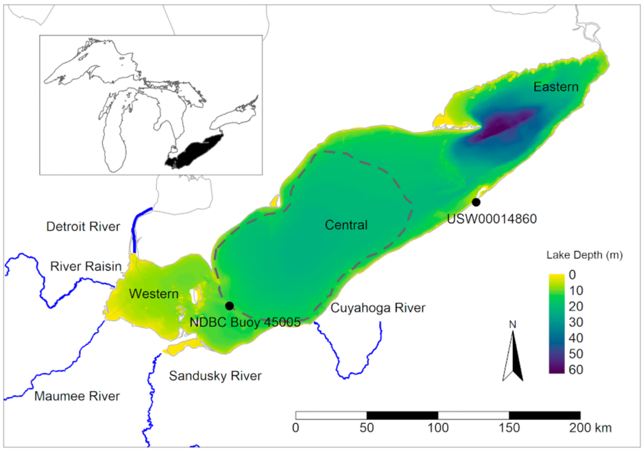

Figure 1. North American Great Lakes, Lake Erie's three basins, NOAA NWS weather station USW00014860, NOAA NDBC buoy 45005, and the five rivers used as a surrogate for the total load to the central basin. The dashed line represents the 20% probability of hypoxic conditions in September 1987–2007 based on estimated maximum monthly hypoxic areas (Zhou et al. 2013).[29]

Observational Data

Western-Basin HABs. The western basin cyanobacteria index was determined using the satellite integration method described by Stumpf et al.[28] which isolates cyanobacteria-specific spectra. Satellite imagery is generally integrated into 10 day composites. We used the yearly maximum 30 day average (derived from three consecutive 10 day composites) for the cyanobacteria index in the western basin, hereafter referred to as CI-30. These updated CI-30 values were provided by the National Oceanic and Atmospheric Administration (NOAA; R. Stumpf, Pers. comm.).

Central-Basin Hypoxia. Areal hypoxia extent estimates (km^2) for 1985–2024 were geostatistically derived from dissolved oxygen monitoring data.[10,29] Most data were collected from 10 fixed offshore stations in the central basin, sampled at approximately 3 week intervals between June and October by the U.S. Environmental Protection Agency (EPA). These were augmented with data from Environment and Climate Change Canada (ECCC) and NOAA's Great Lakes Environmental Research Laboratory.[29] We linearly interpolated daily values between sampling events and calculated the August–September average (a 61 day mean) for each year. Years requiring more than 30 days of consecutive interpolation (1985, 1986, 1991, 1992, 1994, 1995, 2000, 2010, and 2011) were excluded from model calibration, resulting in a modified data set of annual hypoxic area estimates (n = 31). Prior to 1985, we converted annual anoxic area estimates (n = 14)[30] to hypoxic area using a least-squares regression between the hypoxic/anoxic area ratio (R_{ha}) and anoxic extent (A): $R_{ha} = 3.241 \times A^{-0.365}$ ($R^2 = 0.95$). This conversion yielded a total of 45 years of hypoxic area estimates (1959–2024).

Temperature. Mean monthly overlake air temperature (T_a) from 1950 to 2024 was provided by the U.S. Army Corps of Engineers (D. Fielder, Pers. comm.), developed using established historical approaches.[31] Air temperature was used for the hypoxia model due to its longer historical record. For the HAB model, lake surface temperatures (T_l) from 1985 to 2024 were obtained from the NOAA Great Lakes Surface Environmental Analysis. Future air-temperature projections from the Coupled Model Intercomparison Project Phase 6 (CMIP6) were described in Scavia et al.[10] for the Lake Erie watershed. They selected 15 climate models (Table S3) and considered three socioeconomic pathways: SSP1-2.6 "Sustainability," SSP2-4.5 "Middle-of-the-road," and SSP5-8.5 "Fossil-fueled-development." Daily average temperatures were used to calculate average March–April air temperatures for historical (1950–2014), mid-century (2030–2059), and late-century (2070–2099) periods. For the HAB model, we converted future air temperature projections to lake temperatures: $T_l = 10.26 - 0.1778 \times T_a + 0.0787 \times T_a^2$ (R^2 = 0.87), where T_l is the average spring lake temperature and T_a is the March–April average air temperature defined by the climate models from 2000 to 2024. In the HAB model, the beginning month of spring is a calibration parameter t_w, so spring is from t_w to July (see later description).

Maumee River Loads. Daily 1974–2024 TP and DRP loads were downloaded from Heidelberg University's National Center for Water Quality Research (https://ncwqr.org/) for the Maumee River station at Waterville, which is 42 km upstream from the lake.[28] Daily loads were aggregated to monthly values for the HAB model. TP and DRP measurements are used to calculate the bioavailable P load, as defined by the model below.

Central-Basin Loads. Estimates of TP load into the central basin during 1922–1967[32] were based on transfer coefficients associated with the sewered population; runoff from agricultural, urban, and forested areas; and the atmosphere. Estimates after 1967 are based on the Detroit River and four major tributaries. Detroit River loads for 1968–1981 are from Fraser[33] and Yaksich et al.[34] Loads for 1985–1997 were based on linear interpolation of flow-weighted mean concentration and discharge from the USGS gauge at Ft. Wayne (04165710). For 1998–2024, loads were estimated by adding loads leaving Lake St. Clair to those entering the Detroit River.[35] Water-year loads from the four major tributaries (Maumee, Raisin, Cuyahoga, and Sandusky Rivers) were calculated as described above and in Scavia et al.[10] To account for other tributaries in the U.S. and Canada, we divided our 5-river TP load estimates by 0.6, which is the ratio of our loads to the total loads estimated binationally.[36]

Western-Basin HAB Model

The HAB model is a modification of Scavia et al.,[24] now including a temperature term. The basic deterministic form of the model is as follows

$$\mathrm{HAB} = (\beta_w \times W + \beta_L \times L_m) \times (1 + \beta_{Tl} \times T_l) \quad (1a)$$

where the HAB prediction is in units of CI-30, W is the spring bioavailable P (TBP) load from the Maumee River, L_m is the long-term (multiyear) TBP load from the Maumee River, T_l is the spring lake temperature deviation from 10 °C to help center the data. Both the time of L_m and T_l are determined by two calibration parameters, t_L and t_w, respectively (see later description). The βs are model coefficients. Note that there is no intercept coefficient, as preliminary analysis indicated it did not improve model performance, and because we expect the HAB size to be zero when nutrient loading is zero.

https://doi.org/10.1021/acsestwater.6c00002
ACS EST Water XXXX, XXX, XXX−XXX

Table 1. HAB Model Coefficients

coefficient	unit	mean	median	5th percentile	95th percentile
β_w	CI/1000 MT/month	19.06	15.65	1.31	48.55
β_{w2}	CI/1000 MT/month	278.15	274.91	139.83	425.85
β_L	CI/1000 MT/month	26.47	24.63	3.85	55.70
β_{Tl}	1/°C	0.31	0.29	0.06	0.60
t_w	months	2.60	2.59	2.13	3.16
t_L	years	8.97	8.97	8.22	9.71
W_{cp}	MT/month	68	63	45	110
θ		0.12	0.10	0.02	0.31
σ_{base}	CI	1.07	0.98	0.55	1.90
σ_{adj}		1.18	0.98	0.16	2.92
λ_1		0.41	0.41	0.11	0.71
λ_2		0.29	0.23	0.02	0.77

Consistent with Scavia et al.,[24] the model also includes a change in the slope coefficient when the spring TBP load exceeds the change-point loading value, W_{cp}, which is a calibrated model parameter. Thus, for $W > W_{cp}$, the model becomes

$$\mathrm{HAB} = (\beta_w \times W + \beta_{w2} \times (W - W_{cp}) + \beta_L \times L_m) \times (1 + \beta_{Tl} \times T_l) \quad (1b)$$

where β_{w2} is an adjustment of the spring load slope.

The spring TBP load (W) and spring lake temperature (T_l) are averaged across months from t_w through July, where t_w (month) is a calibrated parameter such that the first month may only receive partial weight. Similarly, the number of preceding years (t_L) excluding the current year,used to calculate the average long-term load from the Maumee River (L_m) is also a calibrated parameter, reflecting how long it would take for the lake to fully respond to a change in watershed loading.

The TBP is defined as follows

$$\mathrm{TBP} = \mathrm{DRP} + (\mathrm{TP} - \mathrm{DRP}) \times \theta \quad (1c)$$

where the fraction of non-DRP (TP-DRP) that is available to algae (θ) is estimated by the model.

Model predictions are related to observations within the Bayesian framework as follows

$$t(\mathrm{HAB}_{obs}) \sim \mathrm{Normal}(t(\mathrm{HAB}), \sigma_{base} + \sigma_{adj}) \quad (2)$$

where $t(\mathrm{HAB})$ and $t(\mathrm{HAB}_{obs})$ are the predicted and observed HAB values on the Box−Cox transformed scale.[37] The Box−Cox transformation function, $t(x) = [(x + \lambda_2)^{\lambda_1} - 1]/\lambda_1$, includes transformation parameters λ_1 and λ_2, which were also estimated through the Bayesian calibration. The baseline residual standard deviation is σ_{base}, that is adjusted upward by σ_{adj} for years when only moderate resolution imaging spectroradiometer (MODIS) satellite imagery were available to develop the NOAA HAB observation (R. Stumpf, Pers. comm).

Central-Basin Hypoxia Model

The hypoxia model builds on prior frameworks[10,38] and is represented as

$$\mathrm{AH} = \beta_0 + \beta_c \times L_{CB} + \beta_{T_a} \times T_a \quad (3)$$

$$\mathrm{AH}_{obs} \sim \mathrm{Normal}(\mathrm{AH}, \sigma)$$

where AH is the area of hypoxia (km^2), L_{CB} is the multiyear average TP load to the central basin (including loads passing through the western basin), T_a is the spring average air temperature, the β are model coefficients, AH_{obs} is the observation, and σ is the residual standard deviation based on the observations. The spring time period for calculating T_a is determined by calibrated parameters t_{a1} and t_{a2} (beginning and end, respectively). Finally, t_c is a calibrated parameter,including the current year, reflecting the number of preceding years over which to determine L_{CB}.

Model Implementation and Validation

The models were developed in R version 4.3.3[39] and NIMBLE package version 1.3.0 for Bayesian inference.[40,41] We evaluated model robustness using leave-one-year-out cross-validation where each year's observation was predicted after removing that observation from the calibration data set and recalibrating the model to the reduced data set.

Load Response Curves

Hypoxia and HAB response curves were created under current and future climate conditions across a range of plausible phosphorus loading values. In this study, the current period is from 2020 to 2024. To characterize uncertainties, we randomly sampled (20,000 draws) from the posterior parameter distributions and residual distributions. For each draw, we randomly sampled five years of temperatures from 2000 to 2024, yielding 100,000 simulations per loading level. To compare the current and future conditions, we added the CMIP6 projected temperature increases to the random samples of current temperatures. We summarized the simulation results (i.e., predicted HAB or AH) with mean, 10th percentile, and 90th percentile to create the response curve with quantified uncertainty.

RESULTS

The HAB Model

HAB Model Fit and Covariate Contributions. The Bayesian posterior parameter estimates for the HAB model are provided tabularly (Table 1) and graphically relative to the prior distributions (Figure S1). Predicted HAB sizes (Figure 2) accounted for 83% of the variability in the observational data ($R^2 = 0.83$), and the leave-one-out cross-validation predictions accounted for 74% of observational variability. For comparison, earlier models explained between 76% and 84% without the temperature term.[24,50,51]

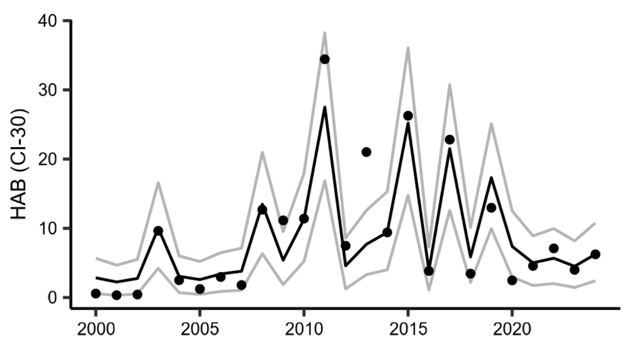

Figure 2. Observed (dots) and predicted (solid back line) with 80% confidence (gray line) intervals of HAB values.

https://doi.org/10.1021/acsestwater.6c00002
ACS EST Water XXXX, XXX, XXX−XXX

We also developed a model evaluating nitrogen (N) and temperature (N replacing P) (Table S4). Consistent with previous research,[27] the N model was not a strong predictor of CI-30 (R^2 = 0.58) compared to the P model (R^2 = 0.83). However, we acknowledge that N may still be critical to HAB management, as it can influence bloom duration[42−44] and toxicity.[45−47] In future studies, it may be advantageous to incorporate both P and N loads to predict peak biomass production.[44,48,49]

HAB Response Curves for Current Climate. The HAB response curve can be conceptualized under different assumptions regarding long-term loading. One approach assumes the long-term load will be altered at the same rate as the spring load (solid line, Figure 3), reflecting a sustained,

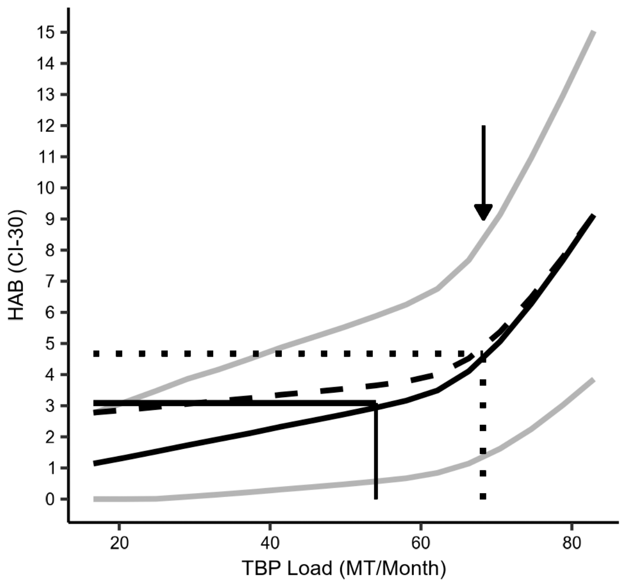

Figure 3. Response of HAB to short-term (dashed line) and long-term (solid lines) total bioavailable loads (MT/month) and the targets of TP and DRP converted to TBP with the 80% credible interval (gray lines). The 2020−2024 load and HAB (68 MT/month, dotted lines) and the target loads (54 MT/month, solid lines) are shown. The arrow indicates the posterior mean of the W_{cp} (68 MT/month), which is the change-point loading value of the model.

"long-term" loading reduction. The alternative approach assumes changes are short-term, with the long-term load remaining at the 2000−2024 average (dashed line, Figure 3). If loading reductions are sustained, it will take approximately 9 years (t_L = 8.97) for the HAB response to fully transition from the short-term to the long-term trajectory.

The current TBP load requires a 21% reduction to meet the target, and it is similar to W_{cp} (Figure 3). Both curves also show that above the loading changepoint (W_{cp} = 68, credible interval = 45−110 MT/month) the marginal effect of loading increases (see eq 1a versus 1b).

At the target load, TBP is 54 MT/month, the model predicts an HAB of 3.1. At the current (2020−2024) load it predicts a HAB of 4.7. In the original analysis (GLWQA 2015), the HAB target corresponded to the mild bloom years of 2004 and 2012, which corresponds to about the 25th percentile of HAB observations. Considering the revised CI-30 data set, the 25th percentile HAB equates to a CI-30 of about 2.9, lower than both of these predictions.

For the HAB model (Figure 4), predictions based solely on load had a standard deviation of 8.74 (CI-30), while

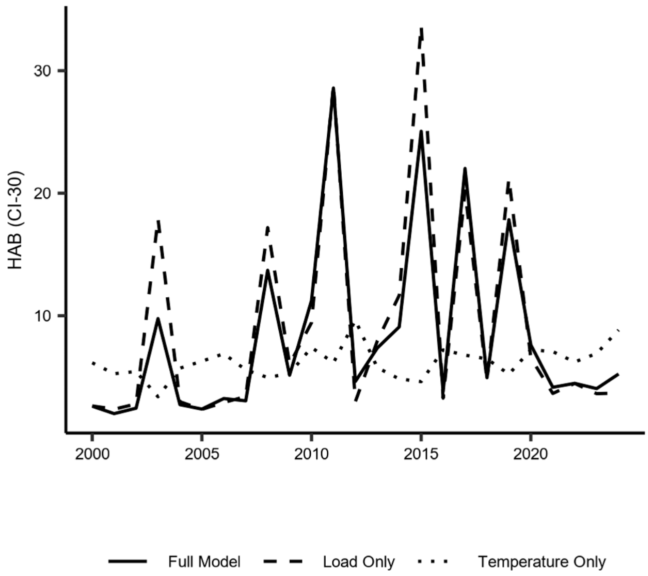

Figure 4. Analysis of HAB model in which nutrient loading and temperature were alternately held constant at their long-term means while the other varied according to the observed annual record.

predictions based solely on temperature had a standard deviation of 1.3, reaffirming that loading remains the primary contributor to HAB severity.

HAB Response Curves for Future Climate. Response curves for future climates used three socioeconomic scenarios that projected temperature increases from the historic baseline to midcentury (2030−2059) and late-century (2070−2099). Projected midcentury temperature increases are 1.4, 1.8, and 2.1 °C and projected late century increases are 1.8, 2.8, and 4.9 °C across the three scenarios. In general, warmer climates yield larger HABs for a given phosphorus load (Table 3). Under the "Middle-of-the-road" scenario (Figure S3), achieving the HAB target requires reducing loads to 42 MT/month by midcentury—a 38% reduction from the 2020−2024 average—compared to a 21% reduction for the current climate. For the HAB model, late century climate requires more reduction.

The Hypoxia Model

Hypoxia Model Fit and Covariate Contributions. The Bayesian posterior parameter estimates for the hypoxia model are provided in Table 2 and Figure S2. The hypoxia model (Figure 5) explained 71% of the observed variability in hypoxic area, with leave-one-out cross-validation explaining 64%. While Scavia et al.[10] reported higher explanatory power (80%) through 2022, they used different loading and extent data sets.

Over the entire simulation period, hypoxia model predictions based solely on load (holding temperature constant) exhibited a standard deviation of 2950 km^2 across time, whereas predictions based solely on temperature had a standard deviation of 1100 km^2. This indicates that, over the last seven decades, nutrient loading has been the primary driver of long-term hypoxia variability. However, during the more recent period (2000−2024), the long-term (∼7 year) loading term has stabilized, reducing the standard deviation associated with loading to only 300 km^2, compared to 1000

Table 2. Hypoxia Model Coefficients

coefficient	unit	mean	median	5th percentile	95th percentile
β_0	1000 km^2	−5.88	−5.51	−11.96	−0.99
β_c	1000 km^2/1000 MT/month	7.81	7.81	6.38	9.2
β_{Ta}	1000 km^2/°C	0.71	0.72	0.36	1.05
t_c	years	7.56	7.33	5.62	10.39
t_{a1}	months	2.39	2.29	1.28	3.83
t_{a2}	months	5.95	5.88	4.08	8.12
σ	1000 km^2	1.92	1.9	1.59	2.33

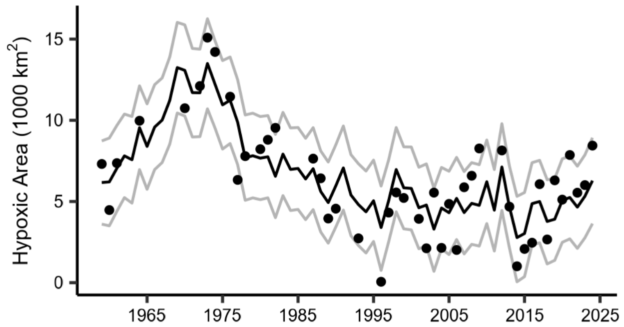

Figure 5. Observed (dots) and predicted (solid back line) with 80% confidence (gray line) intervals of hypoxic area values.

km^2 for temperature (Figure 6). This shift indicates that temperature is now a primary driver of interannual variability.

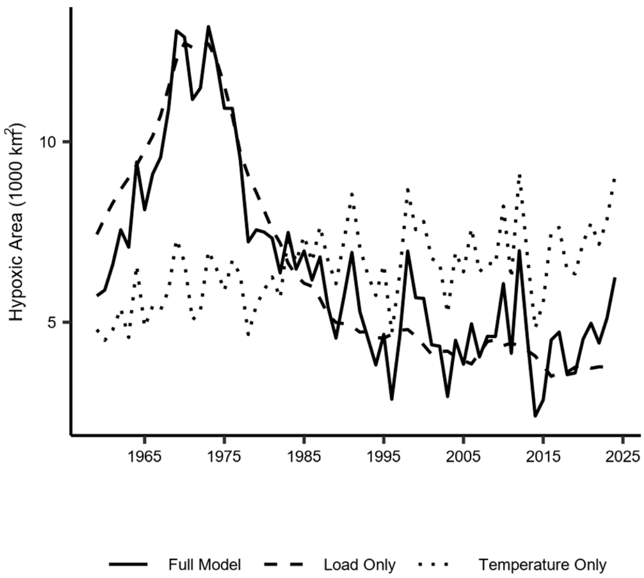

Figure 6. Analysis of the hypoxia model in which nutrient loading and temperature were alternately held constant at their long-term means while the other varied according to the observed annual record.

Hypoxia Response Curves for Current Climate. Because the hypoxia model only incorporates a long-term loading term (eq 3), its response curve inherently reflects sustained changes in loading. This curve indicates a nearly linear relationship between hypoxic area and total phosphorus load (Figure 7). Following loading changes, it takes approximately 7 years (t_c = 7.6, credible interval = 5.62–10.39) with the averaging window including the current year for the central basin to fully respond. The current (2020–2024) mean load is 7296 MT/year (Figure 6, dotted line),

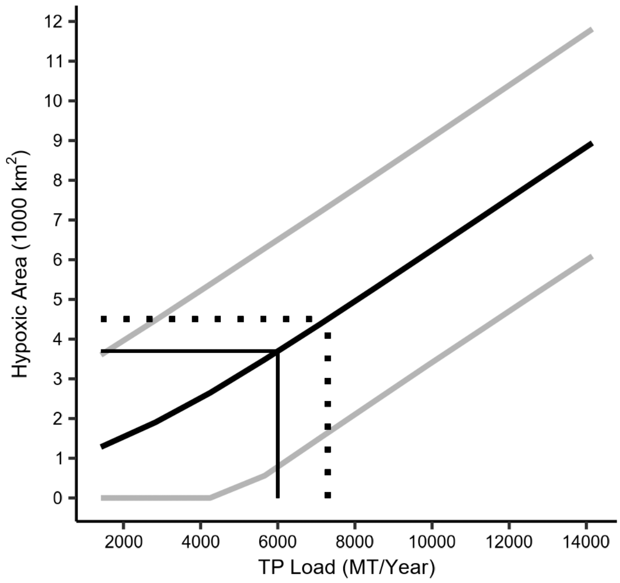

Figure 7. Response of hypoxia (solid black line) and 80% credible interval (gray lines). The 2020–2024 mean load (7296 MT/year, dotted lines) and the target of TP load (6000 MT/year, solid thin lines) the central basin.

which requires a 18% reduction to reach the loading target of 6000 MT/year (solid vertical line).

At the current load, the predicted hypoxic area is 4500 km^2. The binational loading target aimed for an equivalent mean summer hypoxic area of 2500 km^2;[1] however, our updated model predicts an area of 3800 km^2 at that target load. The proposed target corresponds to a hypolimnetic dissolved oxygen concentration of approximately 3.5 mg/L,[2] which is higher than the binationally proposed 2.0 mg/L[1] and aligns more closely with the 4.0 mg/L threshold suggested by earlier modeling efforts.[2]

Hypoxia Response Curves for Future Climate. The hypoxia target (Figure S4) requires a reduction to 4000 MT/year by midcentury, representing a 45% decrease from current loads compared to an 18% reduction at the current climate. In general, warmer climates yield larger hypoxic areas for a given phosphorus load (Table 3). For the hypoxia model, late century climate requires more reduction.

DISCUSSION

Load Reduction and the Effects of Lake Retention

The recent 5 year binational assessment concluded that load reduction targets, which have not changed, are rarely being met.[3] Our loading analysis also suggests that more work needs to be done. From the current loads (2020–2024), a 21% load reduction is needed to reach the HAB target (54 MT/month

https://doi.org/10.1021/acsestwater.6c00002
ACS EST Water XXXX, XXX, XXX−XXX

Table 3. Effect of Climate on HAB and Hypoxia Load Target

HAB load targets need to achieve 3.15 CI-30				
	mid-century		late century	
emission scenario	spring load (MT/month)	reduction (%)	spring load (MT/month)	reduction (%)
SSP1-2.6	44.5	35	40.0	41
SSP2-4.5	42.0	38	37.0	46
SSP5-8.5	41.0	40	30.0	56

hypoxia load targets to achieve 3500 km^2				
	mid-century		late century	
emission scenario	TP (MT/year)	reduction (%)	TP (MT/year)	reduction (%)
SSP1-2.6	4500	38	4000	45
SSP2-4.5	4000	45	2900	60
SSP5-8.5	3500	52	800	89

as TBP), and an 18% central-basin TP load reduction is needed to reach the hypoxia area target (6000 MT/year). There have been some load reductions in the Maumee River since the time when the target was set in 2014. The TBP load in 2014 was about 89 MT/month, requiring a 39% reduction to reach the HAB target. However, most of the load reduction since 2014 is attributable to recent drier hydrologic conditions because flow-weighted mean concentrations (FWMC) remain approximately the same (2014: 0.128 mg/L, 2020–2024: 0.121 mg/L).

The HAB model demonstrates a nonlinear response from a segmented regression with a loading change point (W_{cp}). Other Lake Erie HAB models also show a nonlinear response with nutrient loading.[28,51] Our average W_{cp} is 68 MT/month (Table 1 and Figure 3), which is similar to the inflection point in the HAB model by Hounshell et al.[51] of around 80 MT/month (as TBP).

Based on an examination of Figure 3, we can see that the model's short-term HAB response is nearly as large as the long-term response, indicating that the spring load is more influential than the long-term load in explaining historical variability. While the lake exhibits a substantial immediate response to changes in spring loading (dashed line, Figure 3), our HAB model indicates a significant lag time—approximately 9 years before the system fully equilibrates to watershed loading changes. Similar HAB models by Ho and Michalak[50] and Scavia et al.[24] both identified a 9 year lag associated with DRP and TBP loads, respectively. In contrast, the HAB model in Hounshell et al.[51] suggested that only the current year's spring TBP load is influential.

The time lag (about 7 years) in the hypoxia model represents internal (legacy) storage of nutrients and oxygen-demanding organic material within the lake sediments, which aligns with previous modeling efforts. For hypoxia, Del Giudice et al.[38] estimated a 9 year lag for TP loads from four tributaries, while Scavia et al.[10] suggested a 6 year lag when including the Detroit River. While the statistical models indicating lags have similar deterministic forms, it is encouraging that they continue to identify similar lag periods as they have been updated with revised and extended observational data sets.

Beyond Lake Erie, long-term P loading has been linked to memory effects in European lakes, where a significant fraction of external P is buried and gradually reintroduced.[52,53] Our findings are also consistent with Lake Erie process models[15,54] and experimental studies demonstrating that retained P[55,56] and sediment oxygen demand[57,58] exert a sustained influence over time. This dynamic accounts for both the long-term release of bioavailable phosphorus from sediments and the slow mobilization of more stable phosphorus fractions.[59]

Effects of Climate on the Lake

We evaluated the effects of climate change on Lake Erie's sensitivity to nutrient loading. Under a moderate emissions scenario, increased load reductions are required to meet both hypoxia and HAB targets by mid-to-late century (Table 3). More serious emission scenarios require even more reduction. It is important to note that climate change is also projected to alter the delivery of nutrients from the watershed, which will interact complexly with agricultural management, legacy soil nutrients, and land-use changes.[60−63]

The future warming of lake waters is expected to exacerbate hypoxia.[13,52,58,64,65] In our models, warmer conditions systematically produce larger hypoxic areas, aligning with the results process-based models[14] and empirical observations,[66,67] particularly during years with reduced ice cover and consequently warmer spring waters. While few Lake Erie HAB models explicitly test the effects of climate warming, the need for larger load reductions is consistent with the well-documented physiological advantages that warmer temperatures confer upon algal production,[68] and particularly cyanobacteria.[43,69]

■ CONCLUSION

In this study, statistical models for HABs and hypoxia were refined using extended data sets and new parametrizations. A 21% load reduction is needed to reach the HAB target from the 2020–2024 loads, and an 18% central-basin TP load reduction is needed to reach the hypoxia area target. Once they equilibrate to watershed loading changes, it will take approximately 9 years for HABs and about 8 years for hypoxia to respond. Under moderate emissions, increased load reductions will be required to meet both hypoxia and HAB targets by mid-to-late century. While these statistical approaches rigorously quantify uncertainties, they are inherently correlative. Conversely, process-based models elucidate the mechanistic pathways through which loads and temperatures govern HAB proliferation and hypolimnetic oxygen depletion.[12−14,20] Both modeling paradigms are indispensable for adaptive lake management. Ultimately, synthesizing insights from multiple models[2,70] and employing ensemble approaches[71−73] remains the most robust strategy for guiding policy.

■ ASSOCIATED CONTENT

Supporting Information

The Supporting Information is available free of charge at https://pubs.acs.org/doi/10.1021/acsestwater.6c00002.

> Figures S1 and S2: prior and posterior distributions for the HAB and hypoxia models. Figures S3 and S4: climate effects on HAB and hypoxia models. Tables S1 and S2: inputs and observations for HAB and hypoxia models. Table S3: the 15 climate models used. Table S4: HAB model coefficients with nitrogen as input (PDF)

https://doi.org/10.1021/acsestwater.6c00002
ACS EST Water XXXX, XXX, XXX−XXX

■ AUTHOR INFORMATION

Corresponding Author

Donald Scavia – *School for Environment and Sustainability, University of Michigan, Ann Arbor, Michigan 48104, United States;* orcid.org/0000-0002-2784-8269; Email: scavia@umich.edu

Authors

Yu-Chen Wang – *No. 18, Ln. 8, Hsinchu City 300, Taiwan*
Daniel R. Obenour – *Department of Civil, Construction & Environmental Engineering, NC State University, Raleigh, North Carolina 27695, United States*

Complete contact information is available at:
https://pubs.acs.org/10.1021/acsestwater.6c00002

Author Contributions

All authors contributed to the analysis and writing of the manuscript.

Notes

The authors declare no competing financial interest.

■ ACKNOWLEDGMENTS

This paper was supported in part by grant number 2387 of the Erb Family Foundation. We thank Gang Zhou and Anna Michalak for the analysis of CMIP6 model analysis, Laura Johnson and Nate Manning for the tributary loads, and Yuntao Zhou for her analysis of 2020–2024 hypoxic areas.

■ REFERENCES

(1) GLWQA Task Force. *Recommended Phosphorus Loading Targets for Lake Erie. Annex 4 Objectives and Targets Task Team Final Report*, 2015.

(2) Scavia, D.; DePinto, J. V.; Bertani, I. A multi-model approach to evaluating target phosphorus loads for Lake Erie. *J. Great Lakes Res.* **2016**, *42* (6), 1139–1150.

(3) Annex 4 Adaptive Management Task Team. *Binational Adaptive Management Evaluation for Lake Erie (2017–2021)*, 2023.

(4) U.S. EPA. *Environmental Protection Agency Science Advisory Board Great Lakes Restoration Initiative Action Plan Panel*, 2017.

(5) Stow, C. A.; Rowe, M. D.; Godwin, C. M.; et al. Lake Erie hypoxia spatial and temporal dynamics present challenges for assessing progress toward water quality goals. *J. Great Lakes Res.* **2023**, *49* (5), 981–992.

(6) EPA. *Lake Erie Dissolved Oxygen Monitoring Program Technical Reports*, 2025.

(7) Xu, W.; Collingsworth, P. D.; Kraus, R.; Minsker, B. Spatio-temporal analysis of hypoxia in the central basin of Lake Erie of North America. *Water Resour. Res.* **2021**, *57* (10), No. e2020WR027676.

(8) Tellier, J. M.; Kalejs, N. I.; Leonhardt, B. S.; et al. Widespread prevalence of hypoxia and the classification of hypoxic conditions in the Laurentian Great Lakes. *J. Great Lakes Res.* **2022**, *48* (1), 13–23.

(9) Scavia, D.; Calappi, T. J.; Godwin, C. M.; et al. Wind-Driven Sediment Resuspension in the World's Fourth Largest Lake Contributes Substantial Phosphorus Load to the 11th Largest Lake. *Environ. Sci. Technol.* **2022**, *56* (15), 11061–11070.

(10) Scavia, D.; Ludsin, S. A.; Han, M.; et al. Water quality-fisheries tradeoffs in a changing climate underscore the need for adaptive ecosystem-based management. *Proc. Natl. Acad. Sci. U.S.A.* **2024**, *121* (45), No. e2322595121.

(11) Rowe, M. D.; Anderson, E. J.; Beletsky, D.; et al. Coastal upwelling influences hypoxia spatial patterns and nearshore dynamics in Lake Erie. *J. Geophys. Res. Oceans* **2019**, *124* (8), 6154–6175.

(12) Rowe, M. D.; Valipour, R.; Redder, T. M. Intercomparison of three spatially-resolved, process-based Lake Erie hypoxia models. *J. Great Lakes Res.* **2023**, *49* (5), 993–1003.

(13) Bocaniov, S. A.; Leon, L. F.; Yerubandi, R. R.; et al. Simulating the effect of nutrient reduction on hypoxia in a large lake (Lake Erie, USA-Canada) with a three-dimensional lake model. *J. Great Lakes Res.* **2016**, *42* (6), 1228–1240.

(14) Bocaniov, S. A.; Lamb, K. G.; Liu, W.; Rao, Y. R.; Smith, R. E. H. High sensitivity of lake hypoxia to air temperatures, winds, and nutrient loading: Insights from a 3-D lake model. *Water Resour. Res.* **2020**, *56*, No. e2019WR027040.

(15) Bocaniov, S. A.; Scavia, D.; Van Cappellen, P. Long-term phosphorus mass-balance of Lake Erie reveals a major contribution of in-lake phosphorus loading. *Ecol. Inform.* **2023**, *77*, 102131.

(16) Bocaniov, S. A.; Scavia, D.; Van Cappellen, P. A mass-balance approach for predicting lake phosphorus concentrations as a function of external phosphorus loading: Application to the Lake St. Clair – Lake Erie System (Canada – USA). *Aquat. Ecosyst. Health Manage.* **2023**, *26* (4), 20–30.

(17) Arhonditsis, G. B.; Neumann, A.; Shimoda, Y.; et al. Castles built on sand or predictive limnology in action? Part A. *Ecol. Inform.* **2019**, *53*, 100968.

(18) Arhonditsis, G. B.; Neumann, A.; Shimoda, Y.; et al. Castles built on sand or predictive limnology in action? Part B. *Ecol. Inform.* **2019**, *53*, 100969.

(19) Liu, Q.; Rowe, M. D.; Anderson, E. J.; et al. Probabilistic forecast of microcystin toxin using satellite remote sensing, in situ observations and numerical modeling. *Environ. Modell. Software* **2020**, *128*, 104705.

(20) Verhamme, E. M.; Redder, T. M.; Schlea, D. A.; et al. Development of the Western Lake Erie Ecosystem Model (WLEEM). *J. Great Lakes Res.* **2016**, *42* (6), 1193–1205.

(21) Valipour, R.; León, L. F.; Howell, T.; et al. Episodic nearshore-offshore exchanges of hypoxic waters along the north shore of Lake Erie. *J. Great Lakes Res.* **2021**, *47* (2), 419–436.

(22) LimnoTech. *Development, Calibration, & Application of a Lake Erie Ecosystem Model; Report prepared for U.S. Army Corps of Engineers—Buffalo District*, 2021; p 142 + 6 appendices.

(23) Sinclair, J. S.; Fraker, M. E.; Hood, J. M.; et al. Eutrophication, water quality, and fisheries: a wicked management problem with insights from a century of change in Lake Erie. *Ecol. Soc.* **2023**, *28*, 10.

(24) Scavia, D.; Wang, Y.-C.; Obenour, D. R. Advancing Freshwater Ecological Forecasts: Harmful Algal Blooms in Lake Erie. *Sci. Total Environ.* **2023**, *856*, 158959.

(25) Scavia, D.; Allan, J. D.; Arend, K. K.; et al. Assessing and addressing the re-eutrophication of Lake Erie: Central Basin Hypoxia. *J. Great Lakes Res.* **2014**, *40*, 226–246.

(26) Watson, S. B.; Miller, C.; Arhonditsis, G.; et al. The re-eutrophication of Lake Erie: harmful algal blooms and hypoxia. *Harmful Algae* **2016**, *56*, 44–66.

(27) Stumpf, R. P.; Wynne, T. T.; Baker, D. B.; Fahnenstiel, G. L. Interannual Variability of Cyanobacterial Blooms in Lake Erie. *PLoS One* **2012**, *7* (8), No. e42444.

(28) Stumpf, R. P.; Johnson, L. T.; Wynne, T. T.; Baker, D. B. Forecasting annual cyanobacterial bloom biomass to inform management decisions in Lake Erie. *J. Great Lakes Res.* **2016**, *42* (6), 1174–1183.

(29) Zhou, Y.; Obenour, D.; Scavia, D.; et al. Spatial and temporal trends in Lake Erie hypoxia, 1987–2007. *Environ. Sci. Technol.* **2013**, *47*, 899–905.

(30) Herdendorf, C. E. *Lake Erie Water Quality 1970–1982: A Management Assessment. Clear Technical Report*, 1983.

(31) Hunter, A.; Clites, K.; Campbell, A.; Gronewold, A. Development and application of a monthly hydrometeorological database for the North American Great Lakes—Part I: Precipitation, evaporation, runoff, and air temperature. *J. Great Lakes Res.* **2015**, *41*, 65–77.

(32) Chapra, S. C. Total phosphorus model for the Great Lakes. *J. Environ. Eng. Div.* **1977**, *103*, 147–161.

(33) Fraser, A. S. Tributary and point source total phosphorus loading to Lake Erie. *J. Great Lakes Res.* **1987**, *13*, 659−666.
(34) Yaksich, S. M.; Melphi, D. A.; Baker, D. B.; Kramer, J. W. Lake Erie Nutrient Loads (1970−1980). *J. Great Lakes Res.* **1985**, *11*, 117−131.
(35) Scavia, D.; Bocaniov, S. A.; Dagnew, A.; et al. Detroit River phosphorus loads: Anatomy of a binational watershed. *J. Great Lakes Res.* **2019**, *45* (6), 1150−1161.
(36) EPA-ECCC. Sources of Phosphorus to Lake Erie. 2025, https://www.blueaccounting.org/metric/sources-of-phosphorus-to-lake-erie/#Explore (accessed Dec 9, 2025).
(37) Box, G. E. P.; Cox, D. R. An analysis of transformations. *J. R. Stat. Soc. Ser. B Methodol.* **1964**, *26* (2), 211−252.
(38) Del Giudice, D.; Zhou, Y.; Sinha, E.; Michalak, A. M. Long-term phosphorus loading and springtime temperatures explain interannual variability of hypoxia. *Environ. Sci. Technol.* **2018**, *52* (4), 2046−2054.
(39) R Core Team. *R: A Language and Environment for Statistical Computing*; R Foundation for Statistical Computing, 2025.
(40) de Valpine, P.; Turek, D.; Paciorek, C.; et al. Programming with models: Writing statistical algorithms for general model structures with NIMBLE. *J. Comput. Graph. Stat.* **2017**, *26* (2), 403−413.
(41) de Valpine, P.; Paciorek, C.; Turek, D.; et al. *NIMBLE User Manual*; NIMBLE Development Team, 2024.
(42) Del Giudice, D.; Fang, S.; Scavia, D.; et al. Elucidating controls on cyanobacteria bloom timing and intensity via Bayesian mechanistic Modeling. *Sci. Total Environ.* **2021**, *755*, 142487.
(43) Gobler, C. J.; Di Cecco, G. J.; Doherty, O. M.; Kramer, B. J. Decadal warming has intensified Microcystis-dominated cyanobacterial blooms in Lake Erie. *Limnol. Oceanogr. Lett.* **2024**, *9*, 593−601.
(44) Chaffin, J. D.; Bridgeman, T. B.; Bade, D. L. Nitrogen Constrains the Growth of Late Summer Cyanobacterial Blooms in Lake Erie. *Adv. Microbiol.* **2013**, *3*, 16−26.
(45) Chaffin, J. D.; Westrick, J. A.; Reitz, L. A.; Bridgeman, T. B. Microcystin congeners in Lake Erie follow the seasonal pattern of nitrogen availability. *Harmful Algae* **2023**, *127*, 102466.
(46) Jankowiak, J.; Hattenrath-Lehmann, T.; Kramer, B. J.; et al. Deciphering the effects of nitrogen, phosphorus, and temperature on cyanobacterial bloom intensification. *Limnol. Oceanogr.* **2019**, *64* (3), 1347−1370.
(47) Barnard, M. A.; Chaffin, J. D.; Plaas, H. E.; et al. Roles of nutrient limitation on western Lake Erie CyanoHAB toxin production. *Toxins* **2021**, *13* (1), 47.
(48) Khan, N.; Paerl, H. W.; McCarthy, M. J.; et al. Trends in Maumee River Nitrogen Loads and Their Complex Relationship to Harmful Algal Blooms. *Water* **2026**, *18*, 465.
(49) Paerl, H. W.; Chaffin, J. D.; Cheshire, J. H.; et al. Dual phosphorus and nitrogen nutrient reduction will be more effective than a phosphorus-only reduction. *Limnol. Oceanogr.* **2024**, *69*, 2913−2928.
(50) Ho, J. C.; Michalak, A. M. Phytoplankton blooms in Lake Erie impacted by both long-term and springtime phosphorus loading. *J. Great Lakes Res.* **2017**, *43* (3), 221−228.
(51) Hounshell, A. G.; Johnson, L. T.; Stumpf, R. P. Nutrient and environmental factors regulating western Lake Erie cyanobacterial blooms. *Aquat. Ecosyst. Health Manage.* **2023**, *26* (4), 63−75.
(52) North, M. M.; North, R. L.; Livingstone, D. M.; et al. Long-term changes in hypoxia and soluble reactive phosphorus in the hypolimnion of a large temperate lake. *Global Change Biol.* **2014**, *20* (3), 811−823.
(53) Jeppesen, E.; Søndergaard, M.; Meerhoff, M.; et al. Shallow lake restoration by nutrient loading reduction some recent findings and challenges ahead. In *Shallow Lakes in a Changing World*; Springer, 2007; pp 239−252.
(54) Nürnberg, G. K.; Howell, T.; Palmer, M. Long-term impact of central basin hypoxia and internal phosphorus loading on north shore water quality in Lake Erie. *Inland Waters* **2019**, *9* (3), 362−373.
(55) Matisoff, G.; Kaltenberg, E. M.; Steely, R. L.; et al. Internal phosphorus loading in western Lake Erie. *J. Great Lakes Res.* **2016**, *42*, 775−788.
(56) Paytan, A.; Roberts, K.; Watson, S.; et al. Internal loading of phosphate in Lake Erie Central Basin. *Sci. Total Environ.* **2017**, *579*, 1356−1365.
(57) Godwin, C. M.; Miller, R.; Rowe, M. D.; Stow, C. A.; Johengen, T. H. Seasonally Variable Sediment Oxygen Demand Kinetics in Lake Erie's Central Basin. *JGR, J. Geophys. Res., Biogeosci.* **2026**, *131*, No. e2024JG008689.
(58) Rucinski, D. K.; DePinto, J. V.; Beletsky, D.; Scavia, D. Modeling hypoxia in the central basin of Lake Erie under potential phosphorus load reduction scenarios. *J. Great Lakes Res.* **2016**, *42* (6), 1206−1211.
(59) Lake, B. A.; Coolidge, K. M.; Norton, S. A.; Amirbahman, A. Factors contributing to the internal loading of phosphorus from anoxic sediments. *Sci. Total Environ.* **2007**, *373*, 534−541.
(60) Muenich, R. L.; Kalcic, M.; Scavia, D. Evaluating the impact of legacy P and agricultural conservation practices on nutrient loads. *Environ. Sci. Technol.* **2016**, *50*, 8146−8154.
(61) Ballard, T. C.; Michalak, A. M.; McIsaac, G. F.; Rabalais, N. N.; Turner, R. E. Comment on "Legacy nitrogen may prevent achievement of water quality goals in the Gulf of Mexico". *Science* **2019**, *365*, No. eaau8401.
(62) Ballard, T. C.; Sinha, E.; Michalak, A. M. Long-term changes in precipitation and temperature have already impacted nitrogen loading. *Environ. Sci. Technol.* **2019**, *53*, 5080−5090.
(63) Van Meter, K. J.; McLeod, M. M.; Liu, J.; Tenkouano, G. T.; Hall, R. I.; Van Cappellen, P.; Basu, N. B. Beyond the mass balance: Watershed phosphorus legacies and the evolution of the current water quality policy challenge. *Water Resour. Res.* **2021**, *57*, No. e2020WR029316.
(64) Foley, B.; Jones, I. D.; Maberly, S. C.; Rippey, B. Long-term changes in oxygen depletion in a small temperate lake: Effects of climate change and eutrophication. *Freshwater Biol.* **2012**, *57*, 278−289.
(65) Zhang, Y.; Fu, H.; Chen, H.; Liu, Z. Climate-driven intensification of hypolimnetic deoxygenation in lake Fuxian. *Ecol. Indic.* **2023**, *154*, 110567.
(66) Jansen, J.; Simpson, G. L.; Weyhenmeyer, G. A.; et al. Climate-driven deoxygenation of northern lakes. *Nat. Clim. Change* **2024**, *14*, 832−838.
(67) Beall, B. F. N.; Twiss, M. R.; Smith, D. E.; et al. Ice cover extent drives phytoplankton and bacterial community structure in a large north-temperate lake. *Environ. Microbiol.* **2016**, *18* (6), 1704−1719.
(68) Baird, B. W.; Borah, S. S.; Elser, J. J.; Obenour, D. R. Probabilistic assessment of algal nutrient limitation across lakes, leveraging trends with temperature and depth. *Limnol. Oceanogr.* **2026**, *71* (4), No. e70375.
(69) Paerl, H. W.; Huisman, J. Blooms Like It Hot. *Science* **2008**, *320*, 57−58.
(70) Kujawa, H.; Kalcic, M.; Martin, J.; et al. Using a Multi-Institutional Ensemble of Watershed Models to Assess Agricultural Conservation Effectiveness. *J. Am. Water Resour. Assoc.* **2022**, *58*, 1326−1340.
(71) Scavia, D.; Bertani, I.; Obenour, D. R.; et al. Ensemble modeling informs hypoxia management in the northern Gulf of Mexico. *Proc. Natl. Acad. Sci. U.S.A.* **2017**, *114*, 8823−8828.
(72) Shikhani, M.; Feldbauer, J.; Ladwig, R.; et al. Combining a Multi-Lake Model Ensemble and a Multi-Domain CORDEX Climate Data Ensemble for Assessing Climate Change Impacts on Lake Sevan. *Water Resour. Res.* **2024**, *60*, No. e2023WR036511.
(73) Olsson, F.; Moore, T. N.; Carey, C. C.; Breef-Pilz, A.; Thomas, R. Q. A Multi-Model Ensemble of Baseline and Process-Based Models Improves the Predictive Skill of Near-Term Lake Forecasts. *Water Resour. Res.* **2024**, *60*, No. e2023WR035901.

https://doi.org/10.1021/acsestwater.6c00002
ACS EST Water XXXX, XXX, XXX−XXX